CLM-P809

CLM-P809

UKAEA

Preprint

NUMERICAL SIMULATION OF IDEAL INTERNAL KINK MODES WITH FLAT CENTRAL q PROFILE

P. KIRBY

CULHAM LABORATORY
Abingdon Oxfordshire
1987

NUMERICAL SIMULATION OF IDEAL INTERNAL KINK MODES WITH FLAT CENTRAL q PROFILE

P. Kirby

Culham Laboratory, Abingdon, Oxfordshire, OX14 3DB, UK.
(EURATOM/UKAEA Fusion Association)

ABSTRACT

This paper describes non-linear numerical simulations of ideal internal kink modes in cylindrical geometry with a flat central q profile as a model for the rapid sawtooth collapse seen in large tokamaks. The resulting plasma motion is consistent with that obtained experimentally from X-ray tomographic reconstruction. Attention is drawn to the effects of limited poloidal resolution in this diagnostic.

(Submitted for publication in NUCLEAR FUSION)

1. Introduction

This paper describes a series of non-linear numerical simulations of internal kink modes in cylindrical geometry with a flat central q profile. Its purpose is to investigate the idea that the rapid sawtooth collapse seen in large tokamaks is due to an *ideal* $m=1$ instability[1].

The calculations, carried out with a 3-dimensional incompressible MHD code without transport effects, do not attempt to simulate a train of sawtooth oscillations, but focus instead on the plasma motion that accompanies a single sawtooth collapse. In particular, an attempt has been made to model the distribution of emission that would be seen in experimental X-ray tomographic reconstruction[2] of such motion.

The need to re-appraise the theory of sawtooth oscillations has become apparent from results[3] from large tokamaks which show a sawtooth collapse time (typically 100 μs in JET) much shorter than that (typically 5 ms in JET) suggested by the conventional Kadomtsev model[4], and the frequent absence of any significant plasma perturbation (rotating or stationary) immediately before the collapse.

The idea[1] that the plasma motion during a sawtooth crash is due to the ideal $m=1$ internal mode has been developed in[5]. In this theory, it is argued that owing to the long resistive diffusion time, the q profile can change by only a small amount (typically 1%) during the sawtooth ramp phase. With the assumption that the sawtooth process flattens q to unity in the central region, it follows that q must also be close to unity at the onset of collapse.

Although the hypothesis of a flat central q is eminently plausible and appears to find some justification from experiment[6], other experimental results[7] suggest that it may not be the only possibility. The resolution of this point is at present unavailable.

With a flat q profile, the ideal $m=1$ internal mode may be unstable in a torus for arbitrarily small values of β_p. This contrasts with the conventional case of monotonically increasing q, for which instability is possible only for values of β_p greatly in excess of those obtained experimentally. The plasma flows associated with the instability are of the form of a diffuse convective cell, rather than the rigid shift ('top-hat') of conventional theory. The investigation of these flows is the subject of the present paper.

In order to put the calculations into precise context, it is useful to consider the nature of the sawtooth collapse in further detail. The experimental results[2] show that it may be regarded in two phases.

The first phase, comprising the first $75-300\,\mu$s (depending on discharge) sees the development of a gross radial motion of the plasma core, with helical symmetry around the torus diagnosed to be $m=1, n=1$. Although the distribution of soft X-ray emission changes, the absolute magnitude remains essentially constant. It seems entirely reasonable to regard this phase as the development of a fluid instability and to interpret the changing X-ray pattern as the result of convection of the emission with the plasma. It is this aspect that is addressed by the numerical simulations.

The second phase, comprising a further $25-100\,\mu$s sees the sudden drop of the X-ray emission everywhere and the loss of energy from the central region until a poloidally symmetric final state is reached. The mechanism of this loss, being a transport phenomenon, is outside the scope of the present simulations and is not considered further.

It will be noted that for simplicity, the present calculations are carried out in cylindrical geometry. This approach would be inappropriate for the conventional case of a monotonic q profile, for which the $m=1$, $n=1$ mode shows a significant difference between the cylinder and the torus. However, as has been noted above, for the case of flat q, the toroidal stabilization is largely removed and with it the difference in stability boundary. The plasma motion is then broadly similar in the two cases and use of a cylindrical model is justified. This view is given support by good qualitative agreement with the results of linear[8] and non-linear[9] calculations in toroidal geometry.

The simulation of a sustained series of sawtooth-like oscillations in cylindrical geometry with a flat q profile has been undertaken using a reduced MHD model[10] and more recently using a full MHD model[11].

2. Numerical model

The numerical model is that of 3-dimensional, resistive, inviscid, incompressible MHD in a periodic cylinder. Although it is resistive, the unstable modes are ideal and the resistivity has no significant effect. In dimensionless units, the equations may be written

$$\frac{\partial \boldsymbol{v}}{\partial t} + \boldsymbol{v}.\nabla \boldsymbol{v} = -\nabla p + j \times \boldsymbol{B}$$

$$\frac{\partial \boldsymbol{B}}{\partial t} = \nabla \times \left(\boldsymbol{v} \times \boldsymbol{B} - \frac{\eta}{S} j \right)$$

$$\nabla . \boldsymbol{v} = 0$$

$$\eta = \eta(r)$$

Here, times are normalized to the Alfvén time based on the (minor) radius of the cylinder and the 'toroidal' magnetic field B_z. S is the ratio of resistive diffusion time to Alfvén time and $\eta(r)$ is the resistivity profile. This is a fixed function of r in the model and is determined by the requirement that the equilibrium current profile j_z is not subject to resistive diffusion, i.e. $\eta(r)\, j_z(r) = \text{const.}$

The boundary conditions are those pertaining to an impermeable conducting wall, i.e. $v_r = 0$, $B_r = 0$. A constant electric field E is applied at the wall to drive the equilibrium current.

These equations, containing neither density nor temperature, clearly do not allow the calculation of an intrinsic X-ray emission. However, as has been described above, the present interest is that for which the emission moves with the plasma. In order to model this, the MHD equations have been augmented by the equation of passive scalar convection

$$\frac{\partial A}{\partial t} + \nabla.(\boldsymbol{v}A) = 0$$

in which A represents the magnitude of X-ray emission. Following experimental observations, the emission A is taken to have a Gaussian profile in the equilibrium state.

The model profile for the equilibrium current j_z has been taken as

$$j_z = j_{z0} = \text{const.} \qquad r < r_1$$

$$j_z = j_{z0} \frac{(C - r^2)^2}{(C - r_1^2)^2} \qquad r \geq r_1$$

and the magnetic field $B_z = 1$. This means that q is exactly constant ($q = q_0$) for $r < r_1$ and rises monotonically with continuous derivative for $r > r_1$. This is therefore the simplest model of a flat q profile. Fig.1 shows a typical case. The constant C is introduced to allow a current density at the wall, necessary with

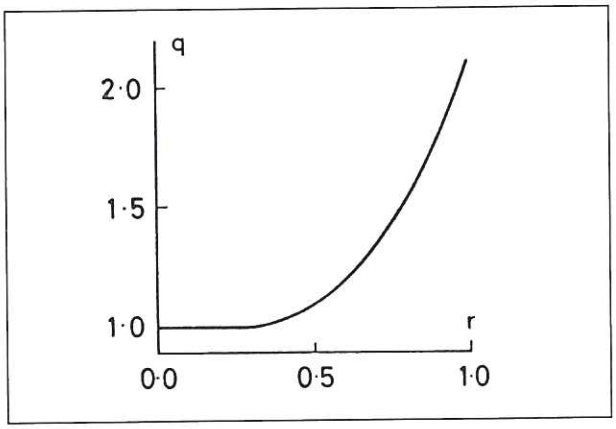

Fig.1 The model q profile. q is constant for $r \leq 0.3$.

an electric field boundary condition. It has been fixed by setting the current density at the wall to be a small fraction (5%) of that at the centre.

In the present calculations, the aspect ratio was 3 and $r_1 = 0.3$ (for consistency with JET), $C = 1.262$ and $1 < q_0 \leq 1.07$. The value of S was taken as 10^5 for numerical simplicity. As has been described above, resistivity makes only a small perturbation to the ideal nature of the instabilities that are found. The numerical representation used poloidal mode numbers $0 \leq m \leq 4$, 'toroidal' mode numbers $-4 \leq n \leq 4$ and 64 radial mesh points.

It is stressed that the simulation uses an equilibrium specified a priori and investigates the consequences of this choice. It is not a self-consistent calculation; in particular the equilibrium is linearly unstable (see below) but the manner of evolution to this unstable state is not addressed.

3. Ideal linear stability of the model equilibrium

In order to clarify the results of the numerical simulations, it is important to investigate the ideal linear stability of the specified equilibrium.

For the incompressible case, the linear eigenvalue equation[12] for the radial displacement $\xi_r(r) \exp i(m\theta + kz)$ in ideal MHD may be written

$$\left[A(r\xi_r)' \right]' - B\xi_r = 0$$

in which

$$A \equiv \frac{r(\gamma^2 + F^2)}{m^2 + k^2 r^2}$$

$$B \equiv \gamma^2 + F^2 - 2B_\theta \frac{\mathrm{d}}{\mathrm{d}r}\left(\frac{B_\theta}{r}\right) - \frac{4k^2F^2B_\theta^2}{(m^2+k^2r^2)(\gamma^2+F^2)} + r\frac{\mathrm{d}}{\mathrm{d}r}\left(\frac{2mFB_\theta}{r(m^2+k^2r^2)}\right)$$

Here γ is the growth rate and $F \equiv mB_\theta/r + kB_z$. The wave vector k is given by $k = 2\pi n/L = n/R$ in which L is the periodic length of the cylinder, R is its 'major radius' and n is the 'toroidal' mode number. Resonant modes have negative n in this convention.

With the conditions $r\xi_r = 0$ at $r = 0$ and $r = 1$, this equation provides a 2-point boundary value problem for ξ_r and γ. This has been solved numerically using the Lentini-Pereyra method[13]. The advantage of such a (finite difference) approach is the availability of a global error estimate and hence the provision of a numerical solution of over all high integrity and accuracy (typically 1 part in 10^5).

Of particular interest is the dependence of the growth rate γ on the parameter q_0, the central value of q. This is shown in Fig.2 for the mode numbers $m/n = -1$, $m = 1,2,3,4$. It can be seen that for a given m number there is a value of q_0 (decreasing with m) below which

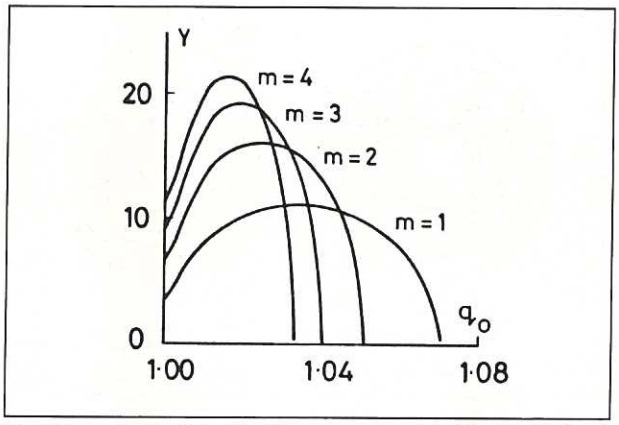

Fig.2 Dependence of the ideal linear growth rate γ (in units $10^{-3}/\tau_A$) on q_0 (the central value of q) for modes $m/n = -1$, $m = 1,2,3,4$.

the mode becomes unstable. It is also apparent that the maximum growth rate increases with m, as $m^{1/2}$.

The features of Fig.2 can be understood in terms of a partial analytic solution of the eigenvalue equation. In the region of constant q, the equation may be solved exactly[14]. The appropriate solution for $m/n = -1$ may be written

$$r\xi_r = mJ_m(\lambda r) - \left(\frac{k^2}{k^2+\lambda^2}\right)^{1/2} \lambda r J_m'(\lambda r)$$

$$\gamma^2 = \left(\frac{B_z}{q_0 R}\right)^2 m^2(q_0 - 1)\left(1 - q_0 + \frac{2}{(\lambda^2+k^2)^{1/2}R}\right)$$

The quantity λ is determined by requiring continuity C^1 with the decaying solution in the region $r > r_1$.

It is clear from these expressions that γ^2 is a near parabolic function of $(1-q_0)$, in qualitative agreement with Fig.2. In addition, the value of q_0 for marginal stability

$$q_0(\gamma = 0) = 1 + \frac{2}{\lambda R}$$

is a decreasing function of m, as observed. This follows because the outer solution is then small, so that λ ($\lambda^2 \gg k^2$) is roughly given by $J_m(\lambda r_1) = 0$ and is therefore an increasing function of m.

A more accurate value for the marginal value of λ for $m = 1$ may be obtained analytically in the limit of large aspect ratio by developing the solution for $r \gtrsim r_1$. In this region, characterized by a length scale δ given by

$$\delta^2 = \frac{2q_0(q_0-1)}{q_1''}$$

the approximate solution for ξ is

$$\xi = \xi_1\left[1 - \frac{2}{\pi}\left(\frac{y}{1+y^2} + \arctan y\right)\right]$$

in which $y \equiv (r - r_1)/\delta$. The expression for λ derived by matching the inner and outer solutions may then be written

$$\lambda \simeq \lambda_0\left(1 - \frac{\pi\delta}{4r_1}\right)$$

in which $\lambda_0 \equiv 3.832/r_1$ is the value of λ obtained by neglecting the outer solution. This shows that the layer $r \gtrsim r_1$ is destabilizing.

It should be noted that γ^2 does not necessarily vanish for $(1-q_0) \to 0$ since $(\lambda^2 + k^2)$ also becomes small and the limiting value must be determined by a full solution.

In fact the value $q_0 = 1$ is special since the perturbed magnetic field $\boldsymbol{b} = \nabla \times (\boldsymbol{\xi} \times \boldsymbol{B})$ is then exactly zero in the region of constant q. Moreover, for the incompressible model, the region becomes neutrally stable, any instability must be driven by gradients in the layer $r \gtrsim r_1$, and the inner eigenfunction for $m = 1$ is a 'top-hat' given by $\xi \simeq 1 + 3k^2r^2/8$. This follows directly from the linearized momentum equation with $\boldsymbol{b} = 0$, $\omega^2\boldsymbol{\xi} = \nabla p$ and the requirement $\nabla . \boldsymbol{\xi} = 0$.

In order to avoid this pathological case, which arises entirely from the assumption of incompressibility, a minimum practical value of $q_0 = 1.005$ has been used in the simulations, rather than $q_0 = 1$ exactly. Fig.3 shows the corresponding eigenfunction for ξ_r.

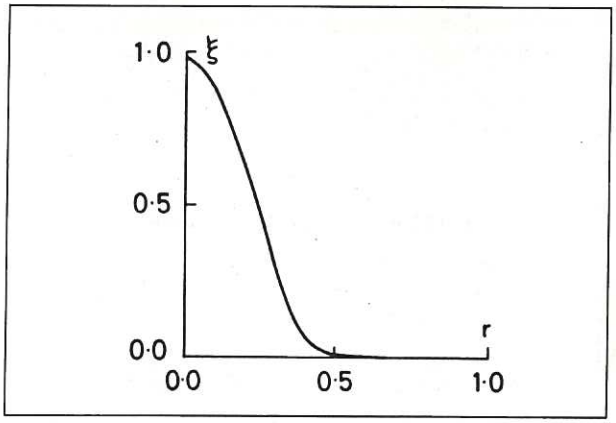

Fig.3 Linear $m = 1$ eigenfunction ξ_r for $q_0 = 1.005$, showing the difference from the 'top-hat' of conventional theory.

The increase of growth rate with m number contrasts with the conventional case of monotonic q, for which modes of higher m number are expected to be more stable, owing to the large positive contribution by the term $(m^2-1)(1-q)^2\xi_r^2$ in the energy principle[15]. However, for the case of small $(1-q)$ this stabilizing term

is clearly diminished and the distinction between $m=1$ and $m>1$ is lost. The feature of growth rate increasing with m is not solely a property of cylindrical geometry but is also apparent in toroidal calculations[16].

4. Simulation results

The existence of a series of unstable modes with $m/n=-1$ means that the precise results of the simulation depend on their relative magnitudes at the start of the calculation. Being motivated here by the study of $m=1$, the initial conditions have been taken as a small perturbation ($\delta B/B \simeq 10^{-6}$) containing only $m=1$, $n=-1$. This means that the higher modes, if unstable, grow from numerical noise at a much lower level ($\delta B/B \simeq 10^{-12}$). It should be noted that a certain arbitrariness has thus been introduced into the simulation model.

Results are presented here for two representative values of q_0, $q_0=1.04$ and $q_0=1.005$. The distinction between them, through the value of (q_0-1), is the decreased effect of field line bending in the latter case compared with the former. This leads to a significant difference in the flow patterns for the two cases.

Fig.4 shows the time development of the poloidal velocity for $q_0=1.04$. The flow is seen to have the form of a diffuse convective cell in the central region. For comparison with experimental values the frames have been annotated with dimensional times, assuming that the normalizing Alfvén time is 0.1 μs (appropriate for JET). A precise numerical comparison is not implied, however. The evolution beyond the time shown in these frames is of no interest for present purposes.

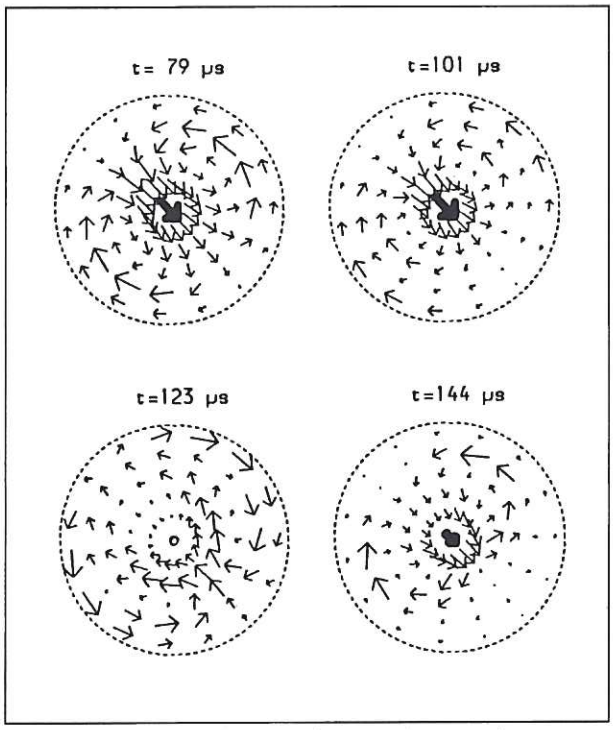

Fig.4 Evolution of poloidal flows for $q_0=1.04$, assuming an Alfvén time of 0.1 μs. The arrows are scaled to the maximum velocity in each frame (respectively 1.5, 1.0, 0.69, 0.73, $\times 10^{-3} v_A$). For clarity, only the region ($r<0.45$) of significant velocity is shown.

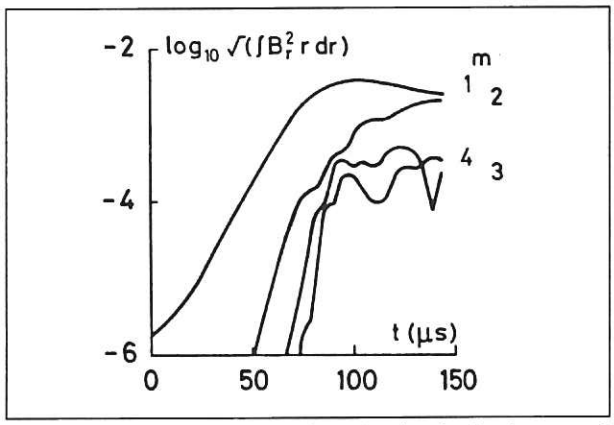

Fig.5 Energy spectrum of B_r vs. time, showing the development of the individual modes for $q_0=1.04$.

Fig.5, a plot of the energy spectrum of B_r (i.e. $\int |\tilde{B}_r|^2 r\mathrm{d}r$) versus time, shows how the individual modes develop for $q_0=1.04$. The dominant mode throughout is $m=1$, with $m=2$ becoming comparable at the end of the run.

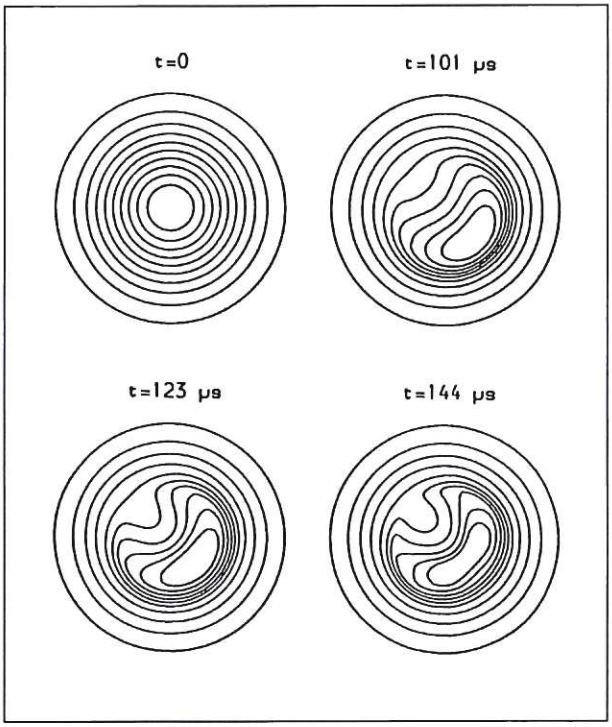

Fig.6 Evolution of contours of simulated X-ray emission for $q_0=1.04$.

Of particular interest is the corresponding evolution of the simulated X-ray emission shown in Fig. 6. The effect of the poloidal flow is to convect plasma from the outer region into the centre. However, for this case of relatively large (q_0-1), the penetration is limited to the formation of a notch in the emission contours. This is rather similar to the tomography results for the partial sawtooth in JET shown in Fig.7.

In contrast, Fig.8 shows the development of the simulated X-ray emission for $q_0=1.005$. The reduced value of (q_0-1) now allows the deep penetration of a cold bubble into the centre of the plasma. In addition, the effect of the more rapidly growing modes of higher

mode number is also apparent in the shape of the contours, particularly $m=4$. This is consistent with Fig.2 which shows that all modes in the calculation are linearly unstable for this value of q_0.

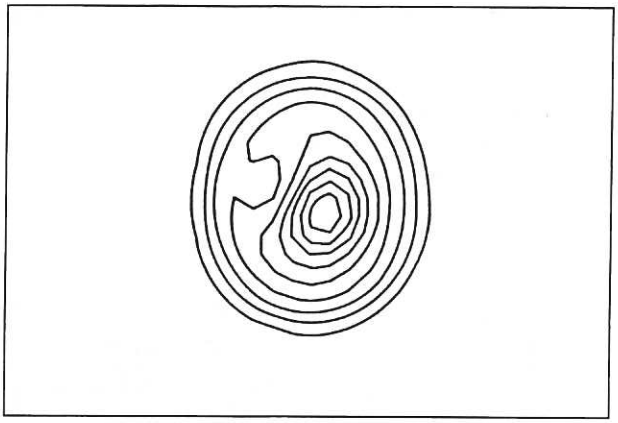

Fig.7 Experimental contours of X-ray emission from a partial sawtooth in JET. (Shot 8898, $t=100\mu s$).

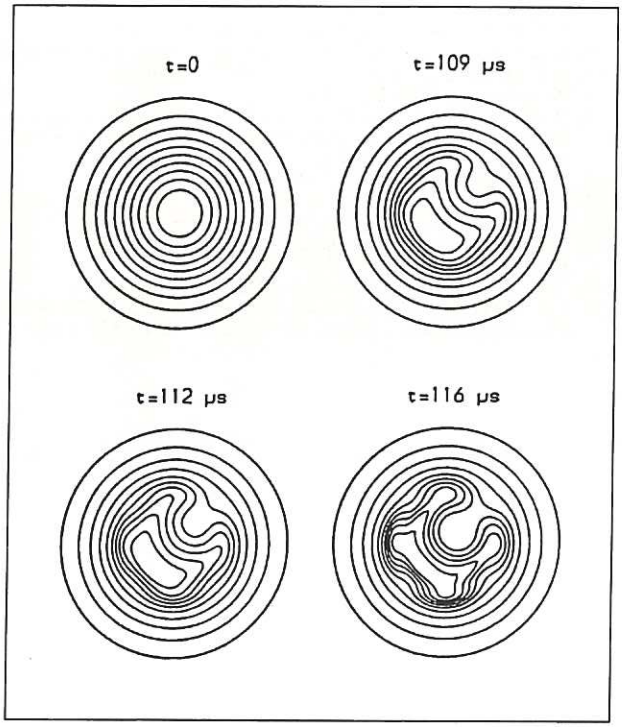

Fig.8 Evolution of contours of simulated X-ray emission for $q=1.005$.

The plot in Fig.9 of the energy spectrum of B_r shows how the individual modes develop for $q_0=1.005$. The linear growth rate of $m=1$ agrees with that in Fig.2 to 3%.

When comparing the simulated X-ray signals with those from JET, it is important to note that the tomographic reconstructions are limited in poloidal resolution to $m\leq 2$ [2]. Fig.10 shows how the simulated X-ray results for $q_0=1.005$ appear when subjected to graphical reconstruction with the same limited poloidal resolution. The penetration of the central region now takes the form of a bubble of cold plasma and is rather similar to the experimental result on JET shown in Fig.11. It should be understood that the appearance in the simulation of this reconnection of the emission contours is entirely an artefact of the reconstruction and that the plot of the actual distribution is shown in Fig.8.

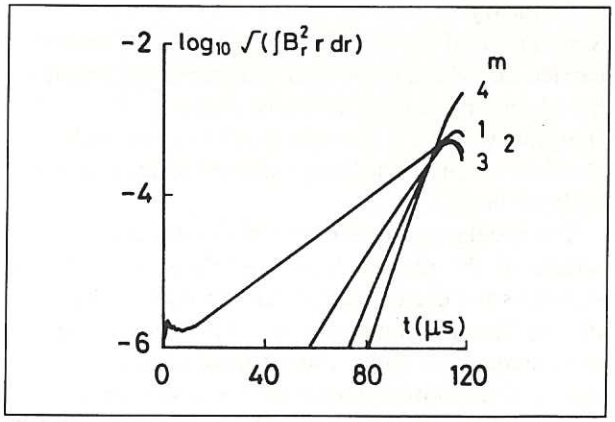

Fig.9 Energy spectrum of B_r vs. time, showing the development of the individual modes for $q_0=1.005$.

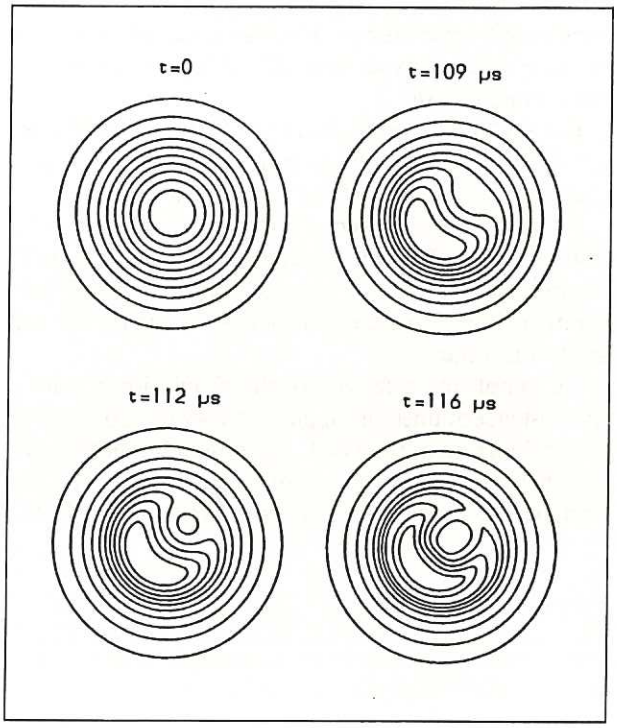

Fig.10 Evolution of contours of simulated X-ray emission for $q_0=1.005$, with $m\leq 2$ in the graphical reconstruction.

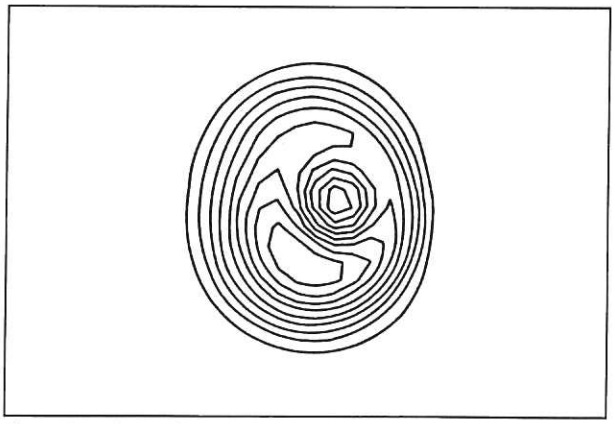

Fig.11 Experimental contours of X-ray emission from a full sawtooth in JET (Shot 9585, $t=75\mu s$).

5. Summary

Simulations of the $m=1$ ideal internal mode have been carried out with a non-linear, cylindrical incompressible plasma model and a simple flat q profile with q marginally above 1. Comparison has been made with the observations of the X-ray emission during a sawtooth collapse in JET.

The calculations are directed specifically at the generic nature of the plasma flows associated with the instabilities and use an unstable equilibrium as initial conditions. The important questions of the evolution to such an unstable state, and of the nature of the loss of energy during a sawtooth collapse are not addressed here.

For a relatively large value of $(q-1)$, the instability is unable to bend the field lines to a great extent and only a small indentation is produced in the contours of the simulated X-ray emission. The results are rather similar to those obtained experimentally in JET for the partial sawtooth collapse.

For a relatively small value of $(q-1)$, the field lines are easily bent and a large region of cold material is convected into the centre of the plasma.

When account is taken of the limited poloidal resolution ($m \leq 2$) in the tomographic reconstruction in JET, the indentation appears as a cold plasma 'island' and is rather similar to the experimental results for the full sawtooth collapse.

A complicating feature of the simulation results is the existence of unstable higher modes with growth rates larger than that of the $m=1$. At present it is not known whether such modes are important in experiment. The evidence from magnetic field measurements on JET is of $n=-2$ and $n=-3$ signals at the plasma edge with amplitudes relative to $n=-1$ of $\simeq 10\%$ and $\simeq 3\%$ respectively[17]. Since the higher modes may be expected to decrease rapidly with distance from the $q \simeq 1$ region, their internal amplitude may in fact be significant. There may therefore be no conflict with the present simulations in this respect.

6. Acknowledgement

It is a pleasure to acknowledge discussions with J. A. Wesson and R. J. Hastie and to thank R. Granetz for providing Figs.7 and 11.

References

1. J.A. Wesson, Plasma Physics and Controlled Fusion **28** 243 (1986)
2. A.W. Edwards et al. Phys. Rev. Lett. **57** 210 (1986)
3. D.J. Campbell et al. Nuclear Fusion **26** 1085 (1986)
4. B.B. Kadomtsev, Sov. J. Plasma Physics **1** 389 (1975)
5. J.A. Wesson, P. Kirby, M.F.F. Nave, Proc. 11th International Conference on Plasma Physics and Controlled Nuclear Fusion Research, Kyoto, paper CN-47/E-I-1-1 (1986)
6. K. McCormick et al. Proc. 12th European Conf. on Controlled Fusion and Plasma Physics, Budapest, Vol.1, p.199 (1985).
7. H. Soltwich, W. Stodiek, A. Kaleck, J. Schluter, U.S. DoE Report DoE/CH/03073-T26 (1985)
8. T.C. Hender, R.J. Hastie, to be published
9. L.A. Charlton et al. Bull. Am. Phys. Soc. paper 7P2 Nov. 1986
10. R.E. Denton, J.F. Drake, R.G. Kleva, D.A. Boyd, Phys. Rev. Lett. **56** 2477 (1986)
11. D. Biskamp, H. Welter, Proc. 11th International Conference on Plasma Physics and Controlled Nuclear Fusion Research, Kyoto, paper CN-47/E-I-1-2 (1986)
12. J.P. Freidberg, Phys. Fluids **13** 1812 (1970)
13. M. Lentini, V. Pereyra, S.I.A.M. J. Numer. Anal. **14** 91 (1977)
14. V.D. Shafranov, Sov. Phys. Tech. Phys. **15** 175 (1970)
15. M.N. Rosenbluth, R.Y. Dagazian, P.H. Rutherford, Phys. Fluids **16** 1894 (1973)
16. T.C. Hender, private communication
17. J.A. Snipes, et al., Proc. 13th European Conference on Controlled Fusion and Plasma Heating, Schliersee, Vol 1, p.152 (1986).